J. Fluid Mech. (1984), *vol.* 147, *pp.* 81–104
Printed in Great Britain

Local measurements in two-phase liquid-metal magneto-fluid-mechanic flow

By PAUL GHERSON AND PAUL S. LYKOUDIS
School of Nuclear Engineering, Purdue University, West Lafayette, Indiana 47907

(Received 24 November 1983 and in revised form 14 April 1984)

Local measurements have been carried out in a mercury–nitrogen two-phase flow using the hot-film anemometric technique, in a cylindrical pipe with electrically insulated walls. The flow was turbulent ($Re = 63000$) and in the bubbly regime ($\langle\alpha\rangle \approx 0.03$). The maximum intensity of the magnetic field was 0.94 T. Processing of the hot-film signal provided in this medium, for the first time, simultaneous quantitative data for the local time-averaged velocity of the liquid-phase turbulent fluctuations, as well as local void fractions. These data were checked against those obtained, for the same conditions, using a double conductivity probe. The latter also provided information on the bubble velocity and average bubble size. Turbulence spectra were also measured.

1. Introduction

The field of magneto-fluid-mechanic (MFM) duct flow is represented by a rich theoretical and experimental literature, for a wide variety of duct geometries and magnetic field orientations. Many comprehensive reviews are available (e.g. Lielausis 1975; Hunt & Shercliff 1975; Reed & Lykoudis 1978; Branover 1978), while the subject is still the focus of international scientific meetings (Hunt & Moreau 1976; Branover *et al.* 1979). A series of excellent monographies (e.g. Ferraro & Plumpton 1966; Shercliff 1975) analysing phenomena specific to the MFM flow (magnetic pressure, ponderomotive force, laminarization effect) are available for the reader who is not expert in MFM. Studies on the magnetic-field effect on a two-phase liquid-metal flow are, however, scarce and – with the exception of the work by Thome (1964) – not older than 7–8 years.

The first investigations were associated with the Liquid-Metal-MFM (LM-MFM) generator project at the Argonne National Laboratory. Thome (1964) studied vertical two-phase flow of sodium–potassium alloy (NaK) and nitrogen in a stainless-steel pipe of rectangular, high-aspect-ratio cross-section. Using a gamma-ray attenuation technique he measured chord-averaged void-fraction profiles upstream and downstream of the magnetic-field region. The direction of traverse was perpendicular to the flow and parallel to the magnetic field. No attempt was made to describe the internal flow structure.

Fabris *et al.* (1980) were the first to use hot-film and resistivity probes in a diverging rectangular cross-section channel† where NaK–nitrogen flowed vertically downwards. Hot-film measurements were taken at the centreline and at two positions closer to the wall, inside the magnetic-field region. The expected decrease in turbulent fluctuation was observed in single-phase flow for increasing magnetic field strengths.

† The characteristic dimensions of the cross-section at the point of measurement were 102 mm × 17.5 mm.

In two-phase flow the magnetic field was reported to decrease the number of detectable bubbles at all positions measured. A paradoxical effect was an apparent increase of the amplitude of the liquid-velocity fluctuations with increasing magnetic-field intensity. This effect, contrary to the well-known damping of the fluctuations observed in single-phase MFM flows, was thought by the authors to be due to the small, 'undetectable' bubbles flowing past the hot-film sensor. Since the size of the hot-film probe used did not allow detection of voids smaller than about 10 mm, their results are mostly qualitative. It should also be mentioned that no turbulent intensities or void-fraction data were computed from the anemometric signal.

Several two-phase LM-MFM investigations have been conducted at Osaka University. Saito (1978) and Saito *et al.* (1978) studied the downward NaK–nitrogen flow in a rectangular stainless steel duct. They reported data on the pressure drop, void distribution and gas–liquid slip ratio. The void-fraction profiles in a direction parallel to the field, measured by a gamma-ray attenuation technique, exhibited two clear maxima at the highest magnetic field (corresponding to an interaction parameter $N = 4.1$).

The first detailed investigation of the local properties of a LM-MFM two-phase vertical pipe flow (Michiyoshi *et al.* 1977) used conductivity probes in a mercury–argon upward slug flow. The authors reported data on void-fraction profiles both parallel and perpendicular to the field direction, bubble-velocity profiles, and histograms of both void velocities and detected chord lengths. The void-velocity profile perpendicular to the field was found to become M-shaped for magnetic fields higher than 0.5 T. The authors did not speculate on the nature of this effect, nor did they attempt to link it to the possibility that similar M-shaped profiles of the liquid velocity might exist: liquid velocity and velocity fluctuation were not measured.

The only data on the liquid-velocity profiles in a liquid-metal two-phase flow are available in the work of Neal (1963). The experiment was conducted in a cocurrent mercury–nitrogen upward flow, in the slug-flow regime. The stagnation pressure measured at the tip of a 3.2 mm diameter cylindrical probe, inserted perpendicularly to the flow, was used to determine the liquid velocity. The probe was connected to a slow-response-time manometer, which smoothed out the fluctuations due to liquid–gas transitions at the probe tip. No magnetic-field effects were studied.

The ratio between the local values of the gas- and liquid-phase velocities (the local slip ratio) is an important parameter of the two-phase flow structure. Its value affects the local void fraction, which, in turn, determines the value of the local electrical conductivity of the two-phase medium. No correlation is presently available for the slip-ratio variation in the cross-section of a liquid-metal two-phase flow, although Neal (1963) presented, in tabular form, data for local velocities of each phase. Slip-ratio profiles have been reported, for water–air two-phase flow, in the extensive work of Serizawa (1974) and Serizawa, Kataoka & Michiyoshi (1975).

The above studies have shown that, in order to understand the complex structure of LM-MFM two-phase flows, data are needed on the local simultaneous values of both liquid and gas phases. Measurements yielding such information have been reported in two-phase pipe flows where magnetic effects are of no concern, using water as the liquid component. Hot-film anemometry was used by Serizawa (1974) to study the local structure of a water–air vertical pipe flow, and also by Lance *et al.* (1980) for bubbly-flow measurements in a test section in which wall effects were insignificant. The laser-Doppler velocimetry (LDV) technique has been used (Theofanous & Sullivan 1982; Ohba & Yuhara, 1979) for extensive measurements of the local turbulent parameters in two-phase vertical pipe flows.

The purpose of the present investigation was to demonstrate the feasibility of

obtaining quantitative data on both phases in a liquid-metal–gas medium, using the hot-film anemometric technique. Such data have not been available before the present work. It is from this perspective that the lack of some desirable features of the experimental facility (e.g. flow development length) and the limited number of flow cases studied, should be considered. The measurements reported below are, in fact, preliminary to an experimental programme at Purdue University's MFM laboratory in which a systematic study of a two-component MFM flow, in an upscaled facility, will be carried out.

2. The experiment

The two-phase mercury–nitrogen loop (see figure 1) consists of a cylindrical Plexiglas test section 127 cm long, with a radius $R = 19$ mm, totally contained inside the gap of the vertical d.c. electromagnet. The mercury was circulated, by means of a rotary pump (Viking K-124, with a capacity of 185 litre/min at a head of 0.5 MPa) through the test section into the separator. Two flexible (bellow) sections prevented the pump vibrations from being transmitted, through the piping, to the test section. The separator consisted of a plastic container in which Plexiglas baffles were mounted in order to allow a better separation of the nitrogen. The latter was vented, through a Tygon pipe, to the atmosphere. From the separator, the mercury flowed downwards, optionally through a bypass filter, into the water-cooled heat exchanger and to the pump inlet. At each end of the test section, a tee junction was mounted, which could accommodate either the nitrogen injector or the probe-traversing mechanism. For the experiments described in this paper, the gas injector was mounted at the bottom (inlet) part of the test section. The injector design used 10 stainless-steel hollow needles connected to an electrical circuit allowing the detection of each bubble released in mercury. The nitrogen flow rate through each needle could be individually controlled. The total flow rate and inlet pressure of the nitrogen were continuously monitored.

The mercury flow rate was measured by a 2.5 cm inner-diameter electromagnet flowmeter using a permanent magnet with a flux density of 0.43 T. The temperature of the mercury was measured using a thermocouple at about 30 cm downstream from the hot-film sensor.

The probe-traversing mechanism, mounted on the upper tee of the test section, allowed the probe to traverse the cross-section along any diameter. A schematic of the scanned cross-section, showing the orientation of the inlet mixing tee with respect to the magnetic field is given in figure 2. For ease of reference, different orientations with respect to the magnetic poles are marked: North, South, East and West. Unless otherwise mentioned, the data reported below have been measured at an axial distance of 112 cm (about 30 diameters) from the inlet of the test section. The whole length of the test section upstream of the measurement point was inside the uniform horizontal magnetic-field region. The distributions of the parameters of interest (local void fraction, liquid mean and fluctuating velocities, bubble velocity and their detected chord length) have been measured along two diameters of the test section: one perpendicular (East–West) and one parallel (South–North) to the direction of the transverse magnetic field. The objective of the experiments was not an extensive study of all two-phase flow regimes; rather, emphasis was placed on the advantages and limitations of the hot-film anemometry for local measurements in a mercury–nitrogen pipe flow.

The experimental runs were conducted at a Reynolds number $Re = 63000$ (based

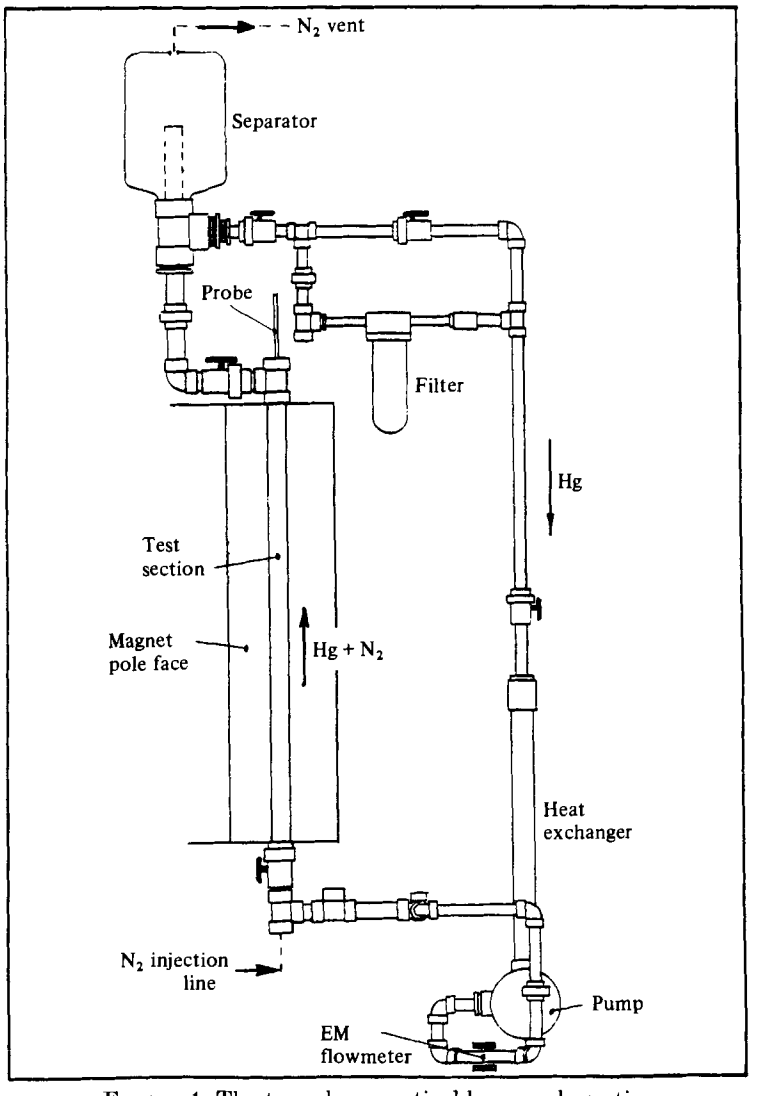

FIGURE 1. The two-phase vertical loop – schematic.

on the liquid superficial velocity). The nitrogen flow rate was kept constant at 16.4 cm^3/s at an injector pressure of 0.39 MPa. For an estimated bubble velocity of about 0.5 m/s, this corresponds to an average void fraction of $\langle\alpha\rangle \approx 0.03$.

The choice of the magnetic-field intensity was dictated by the existence, in single-phase flow, of a 'critical' value of the ratio M/Re of the Hartmann and Reynolds numbers. For M/Re beyond the critical value, the velocity fluctuations in a turbulent liquid-metal pipe flow are suppressed to such an extent as to behave like a laminar flow (the criterion being the friction-factor value). For a duct of circular cross-section the critical value was found (Gardner 1969) to be approximately $M/Re = 4.5 \times 10^{-3}$. The critical Hartmann number for the single-phase mercury flow in our test section would accordingly be $M = 283$, corresponding to a magnetic-field intensity of $B = 0.29$ T. The magnetic-field intensity values chose for our experiment were typically $B = 0$, $B = 0.3$ T and $B = 0.9$ T.

The experiments were carried out at room temperature. The mercury temperature was kept constant (within 0.5 °C) during any particular run.

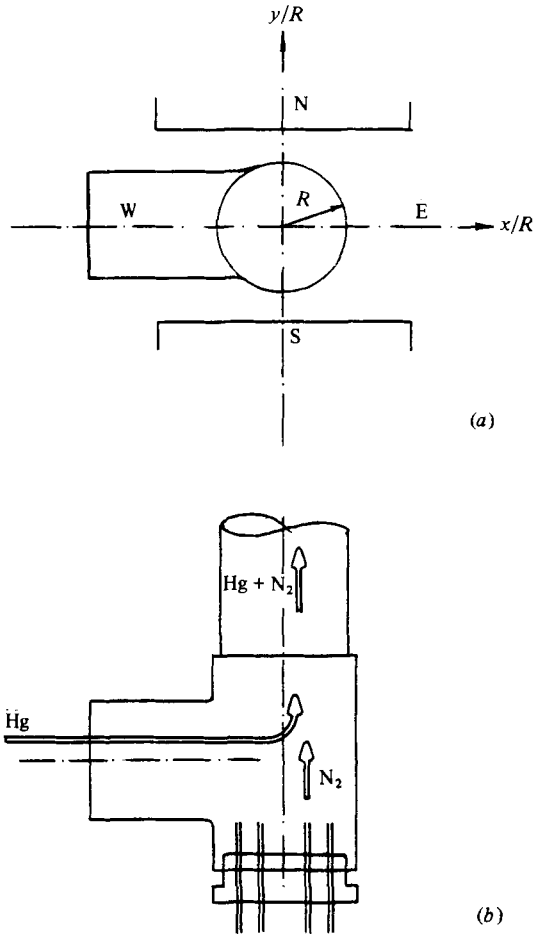

FIGURE 2. Orientation of the test section in the pipe-flow facility: (*a*) cross-section; (*b*) side view of the mixing section.

3. Experimental techniques and data processing

3.1. *Experimental techniques*

Hot-film anemometry was chosen as the measurement technique because the hot-film sensor, besides being sensitive to the flow velocity, can discriminate between the presence of either the liquid or the gas phase at the point of measurement. The method therefore has the potential of yielding simultaneous information on the flow parameters of both phases.

It is well known (see e.g. Lykoudis & Dunn, 1973; Malcolm 1976) that the use of the hot-film anemometry in liquid metals is considerably more difficult than in water or air, mainly owing to the fact that the overall coefficient of heat transfer from the sensor to the liquid metal is readily changed by the deposition of minute impurities, with a lower heat conductivity than the liquid metal, on the sensor surface, leading to a decrease in probe sensitivity.

In a two-phase (mercury–nitrogen) medium we found the above difficulty to be amplified by the fact that, while traversing a liquid–gas interface, the impurities on the sensor surface can trap small gas pockets, which dramatically change the probe sensitivity. Therefore, even after meeting stringent requirements for the cleanliness of both mercury and nitrogen, special data acquisition and processing procedures

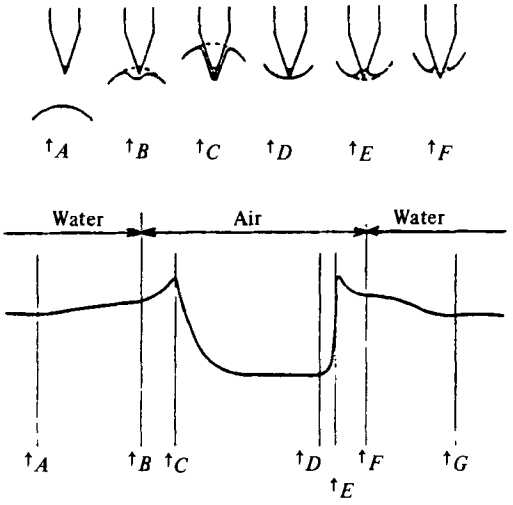

FIGURE 3. Passage of a single air bubble past a conical probe (Delhaye 1969).

(described in more detail in Gherson & Lykoudis 1981) had to be devised in order to handle the occasional probe-sensitivity changes. In essence, these procedures reject the part of the signal in which sudden changes in probe sensitivity are detected.

A miniature conical probe (TSI model 1264-Hg), with a 0.3 mm diameter sensor, was used for the experiments reported below. Cylindrical probes have been ruled out, since the probe geometry allows the formation of a wake retaining gas bubbles whenever a gas–mercury interface is traversed. Wedge-type and conical hot-film probes do not have this drawback. The latter type was chosen for our measurements owing to its better spatial resolution as compared with the wedge-type. An overheat ratio $a = 1.04$ (corresponding to a sensor-to-liquid temperature difference of about 28 °C) was chosen; in previous works using the hot-film technique in single-phase mercury, the practical range of sensor-to-liquid temperature differences has been from 20 to 40 °C (Malcolm 1976).

The response of a hot-film probe during an encounter with a void (the 'void signature') was studied, for an air bubble in water, by Delhaye (1969). Using a simultaneous high-speed ciné camera, Delhaye related the signal pattern to the relative probe–bubble positions (see figure 3). We found the typical signature of a nitrogen bubble in mercury (see figure 4) to be different, in that the transition of the signal from the lower 'gas level' to the higher 'liquid level' is done without the sharp overshoot characteristic to the water–air medium. This difference is due to the much larger wetting angle of mercury ($\gamma \approx 150°$ versus $\gamma \approx 30°$ for water). The time interval between the dewetting and rewetting points (the 'measured' sensor residence time in gas) can be easily determined from the anemometric signal. For air–water this time is an underestimate of the 'real' residence time in gas, which would be obtained if the bubble surface were not deformed. In the case of mercury, on the contrary (see figure 5), the measured residence time in gas is rather an overestimate of the real one, the error depending on the relative size of the sensor versus the bubble size. For the characteristic bubble sizes in our experiment, based on an independent void-fraction measurement using a two-element conductivity probe, this error was estimated to be less than 5%.

The attenuation of the frequency response of the conical hot film probe in mercury (discussed in more detail in Gherson & Lykoudis 1981) was shown not to affect significantly the measured turbulent intensity values. This attenuation (which,

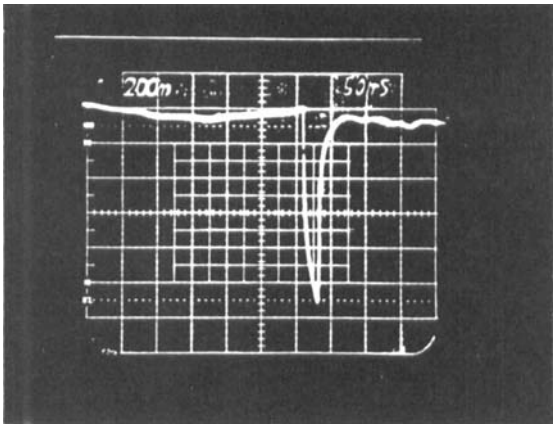

FIGURE 4. Response of the hot-film sensor to a bubble in mercury.

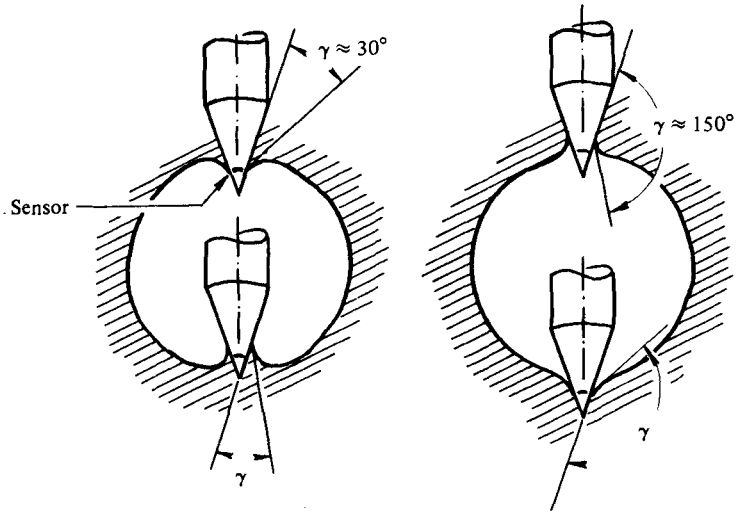

(*a*) (*b*)

FIGURE 5. Surface-tension effects when a hot-film probe traverses a gas bubble: (*a*) in water; (*b*) in mercury.

according to Malcolm & Verma (1981), would be, for our experimental conditions, about 10 % at a frequency of 200 Hz) should, however, be taken into account when turbulent frequency spectra are considered.

The effect of the magnetic-field presence on the probe sensitivity (discussed also in Gherson & Lykoudis 1981) was found to be insignificant, in agreement with the observations of Alemany *et al.* (1979).

3.2. *Data processing*

The output of the anemometric system was digitized and then processed using a PDP11-03 laboratory minicomputer. For every position of the hot-film probe, an ensemble of up to 50 samples of data was taken, containing a total recorded time up to 102.4 s.

Each signal sample consisted of 2048 digitized values, the scanning frequency being 1000 Hz.

3.3. *Computation of the two-phase-flow parameters*

The two-phase-flow parameters computed from the hot-film anemometric data were: (*a*) local, time-averaged, void fraction; (*b*) average detected residence time in gas (ms); (*c*) average number of bubbles detected per sample of signal. All these values were computed for each signal sample then averaged over the ensemble of data.

The local void fraction was determined by computing the ratio of the cumulated residence time of the sensor in the gas phase to the total measurement time. The correspondence between this ratio and the local value of the void fraction was demonstrated by Serizawa (1974).

The detection of each bubble or void in a sample of signal was based on a pattern-recognition technique similar to that proposed by Resch & Leutheusser (1972), based on the comparison of the time derivative of the signal with a threshold value in order to detect interface transitions. It was found that the proposed method failed to detect some of the small bubbles. In order to improve the detection capability, every point in the signal with a level below that corresponding to zero velocity in liquid was artificially assigned a negative value, large enough to provide a drop in the signal of higher magnitude than the threshold. The 'assignment' of negative values was done in the voltage-to-velocity conversion subroutine. The total residence of the sensor in gas was computed by cumulating the time between the signal drop and rise in each bubble signature. The average value of the detected chord length was determined from the average detected residence time in gas, using a bubble rise velocity measured by the two-electrode conductivity probe.

A double-electrode conductivity probe was used to obtain an independent set of data on the void-fraction distribution. Comparing the void fraction profiles measured along the E–W direction using the hot-film probe (figure 8) with those measured using the conductivity probe (figure 9), all the conductivity probe profiles were found to be shifted towards West by a distance of about 0.2 radii (3.8 mm). This shift is probably due to a deformation of the probe support used for the conductivity probe. With this shift accounted for, the profiles measured by the two techniques agree within about 20%. We should also note that the measurements, in two directions – perpendicular and parallel to the magnetic field lines – were taken in different days, and the agreement between the centre-line values of any two corresponding profiles was affected by the use of different calibration curves. For hot-film data this agreement was found to be within the normal scatter of the data (typically 15%).

3.4. *Computation of the liquid-phase parameters*

The processing of the anemometric signal provided (*a*) the mean value and fluctuating intensity of the liquid-phase velocity, and (*b*) the spectrum and autocorrelation function of the fluctuating velocity. Before computing any of the liquid-phase parameters, the part of the signal corresponding to the gas phase was eliminated from the digitized signal. A sample of the signal before and after this removal is presented in figure 6. In this 'bubble clean-up' procedure, it is important to treat correctly the part in the 'signature' of each bubble that is due to surface-tension effects rather than velocity fluctuations of the liquid phase. For the measurements in mercury–nitrogen, where the signal exhibits the characteristic shape shown in figure 4, the gradual rise in the trailing edge of the bubble signature was eliminated from the signal before computing the liquid-phase data, since it is due to the non-wetting of the probe rather than to a liquid-velocity change. The chord 'length' was computed, however, using the point where the signal first begins to rise.

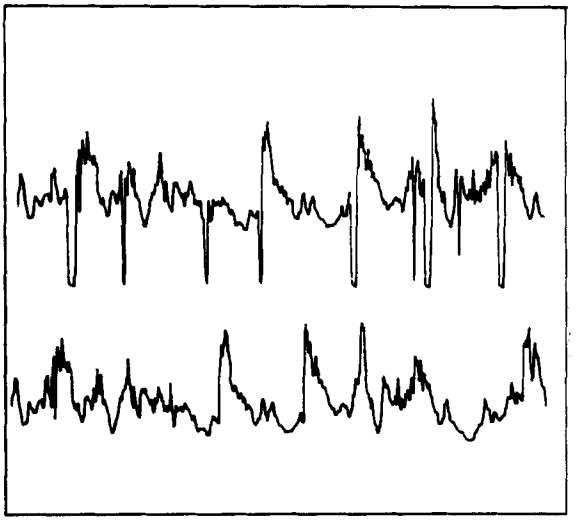

FIGURE 6. Sample of signal (*a*) before and (*b*) after removal of the bubble signatures.

The 'compression' of the liquid-phase signal (figure 6) is likely to affect the shape of the autocorrelation function $R(\tau)$ and the computed spectral distribution $F(f)$. A similar problem has been addressed by Resch & Abel (1975), who compared the Fourier transform of a continuous signal with that of the same signal from which 'observations were randomly missing', and found it to be lower, in the second case, by a fraction approximately equal to the ratio: (missing observation time)/(total observation time), as long as this ratio was small. This ratio would correspond with the void fraction, in a two-phase anemometric signal in which the gas phase has been assigned zero values. For such a signal, we should expect the power spectrum (obtained by squaring the Fourier-transform values for each frequency) to be lower than for a continuous signal, the ratio of the corresponding power-spectral values being of the order $(1-\alpha)^2$.

In order to check what is the effect of a further 'compression' of the signal by eliminating the gas-phase part, we have computed the power spectrum and auto-correlation, first assigning to the 'bubbles' zero values in the anemometric signal, then removing these zero-valued sections from the signal. The difference found in both the autocorrelation and power-spectral density for the low void-fraction value in our experiment was insignificant.

We shall now examine below the influence of the magnetic field on the flow pattern.

4. Data analysis

Before the presentation of the two-phase (mercury-nitrogen) flow pattern and its changes due to the magnetic field, it seems appropriate to provide, as reference, a short description of the single-phase (mercury) flow under the same conditions. Mean-velocity and relative-turbulent-intensity profiles for $B = 0$ and $B = 0.3$ T measured with the conical hot-film probe are shown in figure 7. The magnetic field is seen to reduce the turbulent fluctuations over the whole cross-section, by a factor of roughly 2.5, but has little effect on the mean-velocity profile. Zero-field data in a vertical cylindrical pipe (Gardner 1969) are plotted for reference. For further data on MFM effects in a single-phase mercury pipe flow, the reader is referred to the extensive investigation of Gardner & Lykoudis (1971).

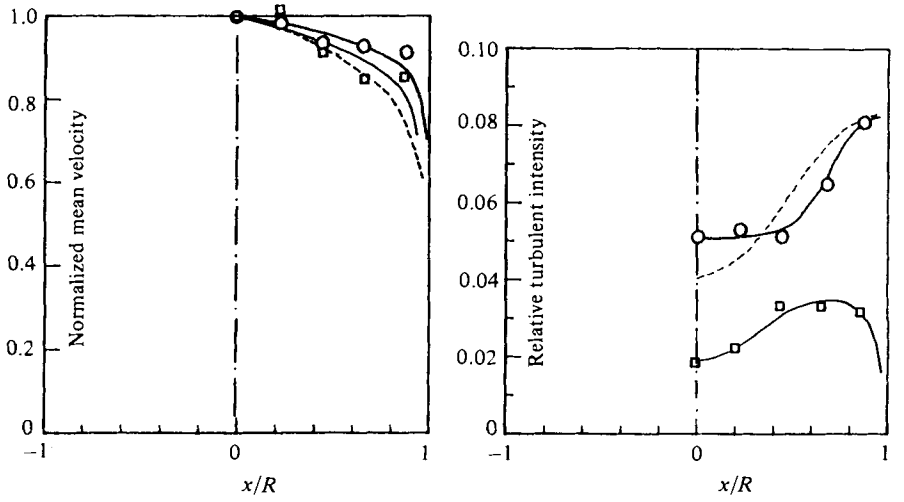

FIGURE 7. Mean-velocity and relative turbulent-intensity profiles in single-phase flow. B (T): ○, 0; □, 0.3. ----, Gardner (1969), $Re = 52000$, $B = 0$.

4.1. *Profiles of the local void fraction*

The void-fraction profiles for zero magnetic field (figures 8 and 9) were found to be dome-shaped in both the (North–South) N–S (y) and (East-West) E–W (x) directions. The North–South direction is in the direction of the magnetic field. The agreement with the profile reported by Neal (1963) for mercury–argon flow at a similar Reynolds number and average void fraction ($Re = 70000$, $\langle\alpha\rangle = 0.05$) is seen to be satisfactory.

The application of a magnetic field $B = 0.3$ T corresponding to the single-phase critical 'laminarization' value, was found to bring about a dramatic change in the void profile, the latter exhibiting a sharp maximum in the (x) E–W direction about $x/R = 0.8$. When the magnetic field intensity was increased to $B = 0.9$ T, the profile recovered its dome shape, although it become flatter along the N–S direction (parallel to the field) than along the E–W direction. We shall discuss this phenomenon after completing the picture of the flow pattern with presentations of the related profiles of liquid and gas phase velocities.

4.2. *Profiles of time-averaged and fluctuating liquid velocity*

The time-averaged liquid velocity U exhibited flat profiles in both directions, in the absence of the magnetic field (see figure 10). A velocity profile reported by Neal (1963) for a slightly higher void fraction (also plotted in figure 10) as well as Serizawa's (1974) profiles in water–air, for $Re = 62000$ and $\langle\alpha\rangle = 0.05$, show the same general shape.

When the magnetic field $B = 0.3$ T is applied, the E–W profile develops a strong asymmetry, well correlated with the corresponding void-fraction profile. For $B = 0.9$ T the profile recovers its almost-symmetrical dome shape. The velocity profile in the (y) N–S direction (parallel to the magnetic-field lines) remains essentially flat for all the values of B, reminiscent of the flat profiles obtained, for the same orientation, in single-phase MFM flows.

The r.m.s. values of the turbulent liquid-velocity fluctuation u' are presented in figure 11. The salient feature of these profiles is their much higher level as compared with corresponding (same Re) single-phase measurements. In the absence of the magnetic field the liquid-velocity fluctuations are 5 times more intense in the core of the flow than the fluctuations measured in single-phase flow (presented for

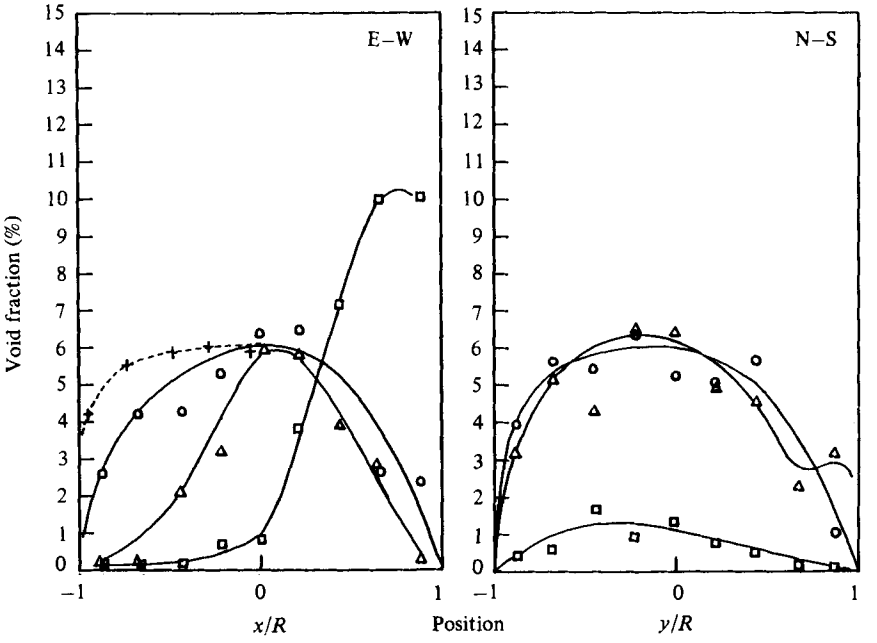

FIGURE 8. Profile of the local void fraction (hot-film). B (T): ○, 0; □, 0.3; △, 0.9. +: Neal (1963), $Re = 70000$.

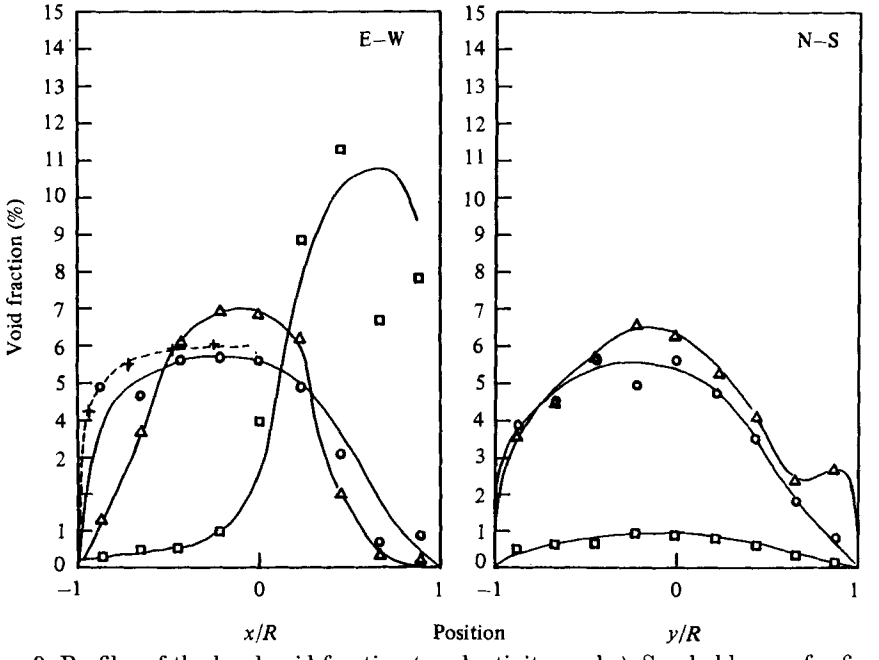

FIGURE 9. Profiles of the local void fraction (conductivity probe). Symbol key as for figure 8.

reference in figure 11). A similar increase in the liquid phase turbulent fluctuations was reported by Serizawa *et al.* (1975) and Theofanous & Sullivan (1982). The former used the hot-film anemometry technique in a vertical cocurrent air–water pipe flow, while the latter data were obtained in a similar test section, but using the laser-Doppler technique and nitrogen–water flow. Theofanous & Sullivan's data are substantially

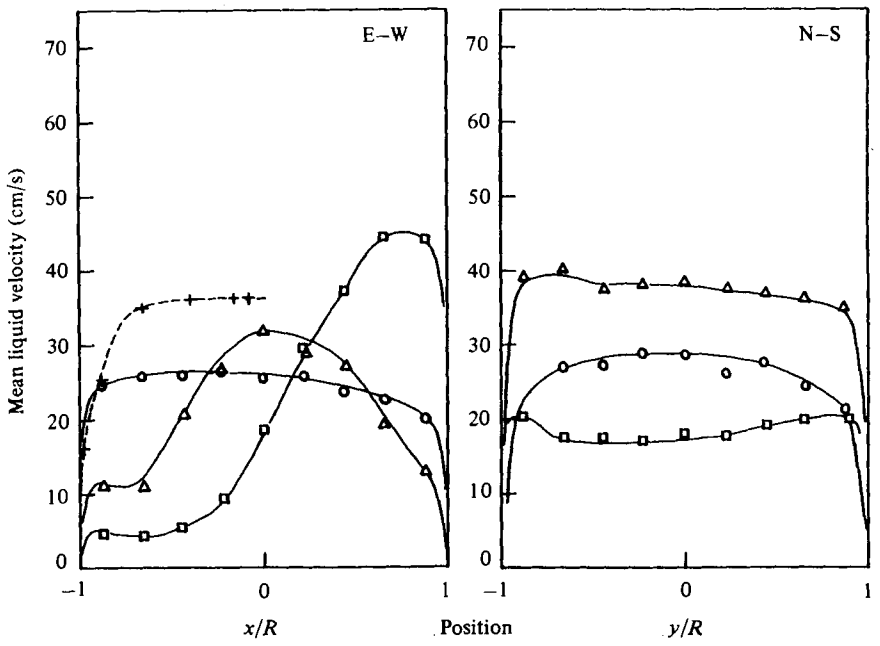

FIGURE 10. Profiles of the mean liquid velocity (hot-film). +, Neal (1963), $Re = 65000$; other symbols as for figure 8.

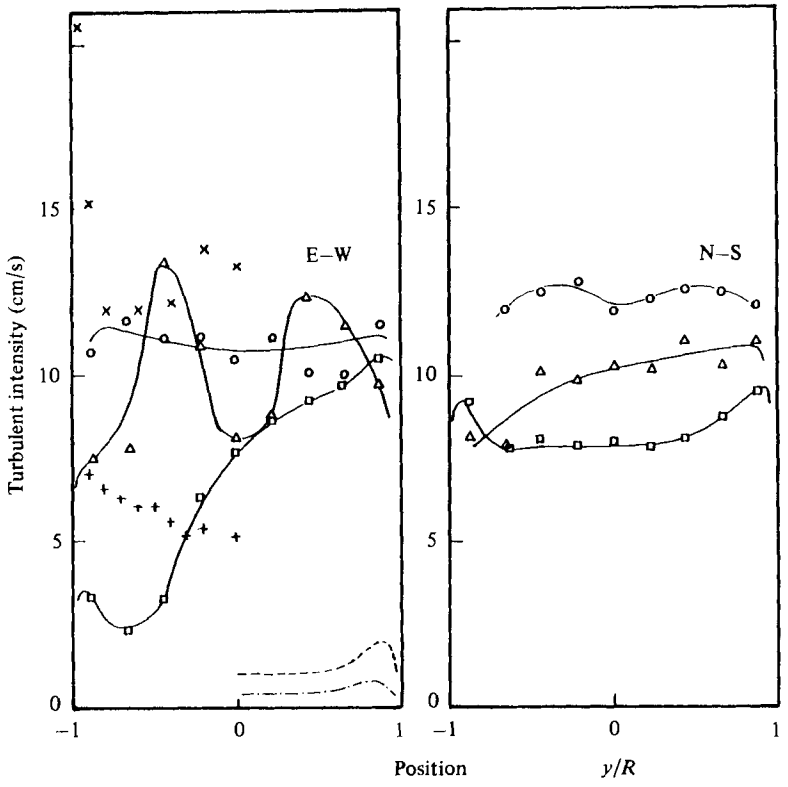

FIGURE 11. Profiles of the turbulent intensity (hot-film). ×, Theofanous & Sullivan (1982), $Re = 21000$, $\alpha \approx 0.038$; ——, single phase, $B = 0$; —·—, single phase, $B = 0.3$ T; other symbols as for figure 8.

higher than those of Serizawa, in particular very close to the wall at a distance of $0.05R$ (see our figure 11). Accordingly, they have taken issue with Serizawa's conclusion that there are no large turbulent-intensity peaks close to the wall, since Serizawa's measurements were limited to a distance higher than $0.10\ R$. Our closest data to the wall were at a distance of $0.12\ R$, as can be seen in figure 11. We doubt very much whether the intensity would be much higher, even if we had approached the wall more closely. The reason for this is that in our experiments we observed that a large number of bubbles attach themselves to the wall, forming a slow-moving layer rather than a fast one. It follows that in two-phase flows it is important to consider the possible influence of a three-phase problem involving the simultaneous interaction of the solid, liquid and gaseous phases, for all measurements made at a distance from the wall of the order of the bubble size, which in all of the above experiments, including ours, was of the order of $0.1\ R$. Equally well, bubble entrance effects and development need to be considered along with the purity of all three phases. When experiments are reported from identical test sections, one needs to be aware of all of the above effects before meaningful comparisons can be made.

We now turn to the data obtained in the presence of the magnetic field.

In single-phase mercury flow, a transverse magnetic field corresponding to a value $M/Re = 4.5 \times 10^{-3}$ was shown (Gardner 1969; Gardner & Lykoudis 1971) to suppress the turbulent-fluctuation intensity to a very low level (about 10 % of the no-field value for $x/R \approx 0.9$ and about 20 % at the centreline). A further increase in the magnetic field intensity did not cause any significant change. (As we have mentioned in §2, the ratio $M/Re = 4.5 \times 10^{-3}$ corresponds, for our test section, to a magnetic field $B = 0.29$ T.)

In the two-phase flow, the picture is found to be completely different. At $B = 0.3$ T, although turbulent-velocity fluctuations are everywhere lower than the no-field level, the relative turbulent intensity in the region $-1 < x/R < -0.5$ is higher than the no-field value; this is due to fast-rising bubbles ($U_b \approx 50$ cm/s) in a region of low mean liquid velocity ($U_m \approx 5$ cm/s).

At the strongest magnetic field ($B = 0.9$ T), we find regions with liquid turbulent fluctuations paradoxically higher than the no-field values. These regions ($-1 < x/R < -0.5$ and $0.5 < x/R < 1.0$) of high turbulent intensity may be regarded as evidence for the bubble break-up phenomenon described at the end of this section.

4.3 *Bubble-size and bubble-velocity distributions*

A further insight into the flow-pattern structure is allowed by the bubble-velocity and bubble-size profiles, measured with the double conductivity probe. The distribution of the bubble sizes is represented (figure 12) by the average value L_b of the detected chord length; the average values of the bubble velocity at different locations across the test section are shown in figure 13.

For zero magnetic field, the average bubble size seems to be larger in the proximity of the walls. At $B = 0.3$ T the asymmetry detected in the void fraction is seen to be correlated with a significant increase in bubble size, for $x/R > 0.5$, evidence of bubble coalescence in this region. Finally, the recovery of the axial symmetry is apparent in the profiles for $B = 0.9$ T.

The average values of the bubble velocity (see figure 13) in the absence of the magnetic field exhibit maxima near the wall, similar to the maxima observed in the bubble size profiles. The higher slip ratio detected in these regions (see figure 14) explains why, although the bubble size is larger near the walls, no maxima appear in the void-fraction profiles at the corresponding locations.

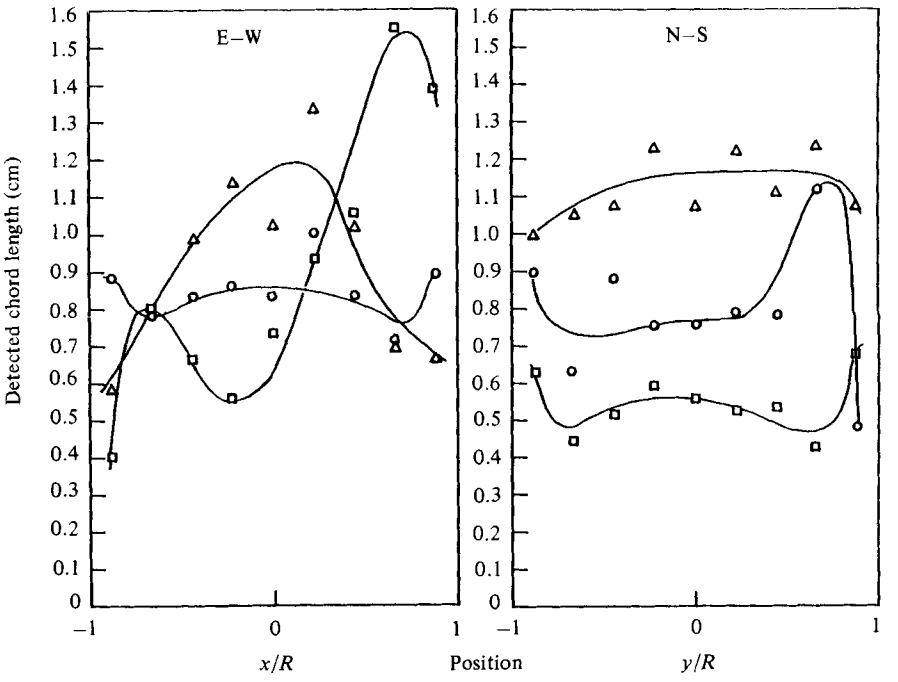

FIGURE 12. Profiles of the detected chord length (conductivity probe). Symbols as for figure 8.

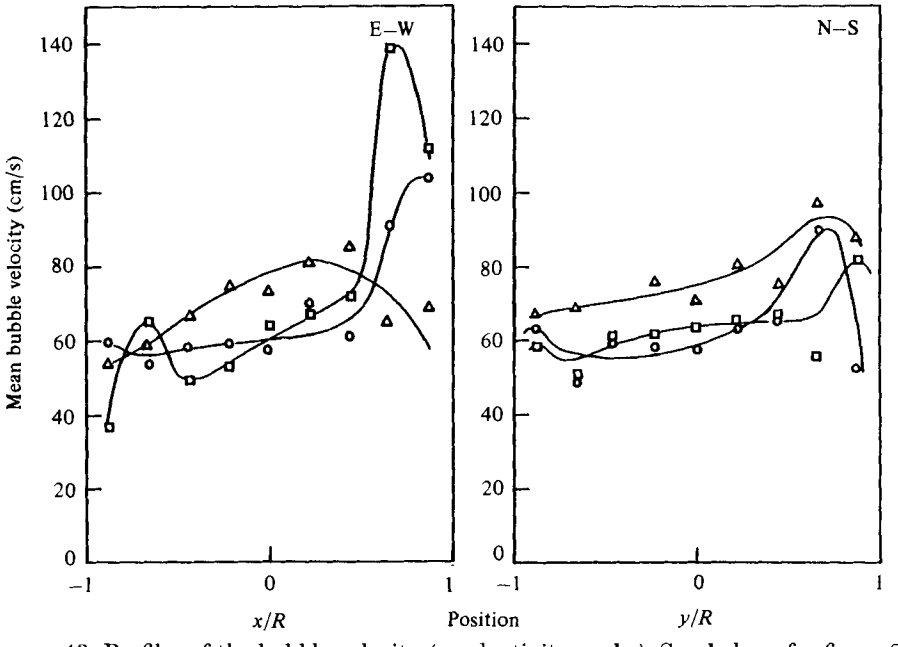

FIGURE 13. Profiles of the bubble velocity (conductivity probe). Symbols as for figure 8.

The application of a magnetic field $B = 0.3$ T enhanced the bubble-velocity maxima near the walls, in particular for $x/R > 0.5$. Finally, for $B = 0.9$ T no sharp velocity maxima were detected. It is interesting to note that the presence of a transverse magnetic field can increase the relative bubble velocity $U_b - U_l$ and the local values of the slip ratio $S = U_b/U_l$ to extremely high values (see figure 14 for

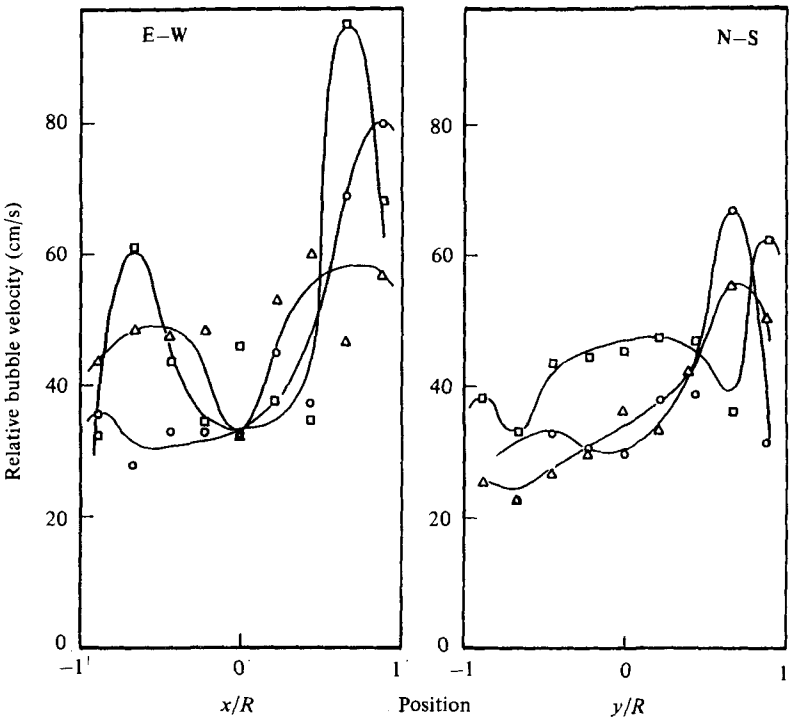

FIGURE 14. Profiles of the relative bubble velocity $U_b - U_l$. Symbols as for figure 8.

$B = 0.3$) T. U_b and U_l are the bubble and liquid-phase velocities. We should note, that near the wall, where the liquid velocity is very low ($U_l \approx 4$ cm/s for $s/R < 0.5$), S can reach values as high as ≈ 15.

We shall now attempt to explain the structural flow developments described above. The first surprising phenomenon observed was the asymmetry in the E–W void-fraction profile brought about by imposing, on the flow, a magnetic field $B = 0.3$ T. The ponderomotive forces acting on an electrically conductive fluid in a circular pipe, due to the interaction with an externally imposed transverse magnetic field, are known to be axially symmetric about a plane passing through the pipe centreline and parallel to the field. Therefore the cause of the abovementioned asymmetry has to be sought in an initial inhomogeneity of the two-phase flow mixture. Indeed, in the mixing tee at the entrance of the test section (see figure 6), the liquid phase entrained the bubbles towards the positive side of the x-axis, overcoming the opposing effect of the centrifugal force acting on the mercury (the latter tends to move the lighter phase towards the negative x-axis). In the absence of the magnetic field, the mixing due to the random agitation of the rising bubbles was sufficiently strong to 'smooth-out' this asymmetry at the point of measurement (30 diameters downstream), except for the bubble velocity profile, which show higher values in the N–E quadrant of the cross-section.

The application of a transverse magnetic field $B = 0.3$ T (which, in our case, corresponds to the critical 'laminarization' value in single-phase flow) is likely to suppress the wobbling motion of the rising bubbles, and, by that, to reduce the bubble dispersion across the flow in a direction perpendicular to the magnetic field. A similar effect was observed by Mori, Hijikata & Kuriyama (1976) for a single bubble rising in a mercury pool: the magnetic field was shown to change the spiraling trajectory

into a rectilinear upward movement. In the same paper, the authors report that, for bubbles of 3 mm or more in diameter, the presence of a magnetic field transverse to the direction of motion lead to a decrease in bubble-rise velocity. In our pipe-flow experiment this effect appears to be masked by the restructuring of the void distribution and bubble size by the field. We note, however, that in the core of the flow (see figures 12 and 13), in spite of an increase of the average void size by a factor of roughly two for $B = 0.9$ T, the corresponding increase in bubble velocity is only about 30 %, and no increase in the relative bubble velocity (figure 16, at the centreline) was detected.

The suppression of bubble dispersion by the magnetic field confines the bubbles to a region (near $x/R = 1$) where they have been entrained in the mixer, thus increasing significantly the void fraction in this region. The higher bubble density leads to an increased rate of bubble coalescence, as witnessed by the maximum near $x/R = 1$ in the bubble-size distribution (figure 12). The larger, faster-rising bubbles impart to the entrained liquid a velocity much higher than the cross-section average (see figure 10). The same effect of the magnetic field on the bubble dispersion is apparent in the void-fraction profiles reported by Michiyoshi *et al.* (1977) for a stream of bubbles injected, from a single nozzle, near the wall of a vertical pipe. Their results showed that the bubble diffusion is suppressed preferentially in the direction perpendicular to the magnetic field. The magnitude of the latter corresponded in their experiment to a ratio $M/Re = 3.0 \times 10^{-3}$.

In order to understand the nature of the changes in the flow structure described above, especially at the high magnetic-field values, additional measurements were carried out: using a longer probe support, a diameter perpendicular to the magnetic field was scanned, at a distance of only 19 diameters from the test-section inlet, using the hot-film probe. The data revealed the same flow pattern as that presented in figures 8–11. However, owing to significant vibration of the probe support, the results are considered only qualitative and are not presented here. We note, nevertheless, that no M-shaped liquid velocity profiles were detected at this location either.

A further series of measurements was performed at 30 diameters from inlet; this time, the magnetic field intensity was changed in smaller increments. The results are presented in figures 15–17. For $B = 0.085$ T almost no magnetic-field influence can be noticed. At $B = 0.21$ T the large scatter seems to indicate an intermittency effect, preceding the transition to the stable profile measured at $B = 0.33$ T. Intermittency was characterized by periods of 'high bubble density' alternating with periods when no bubbles were detected.† A similar intermittency is known to accompany the laminarization, by the magnetic field, of a single-phase MFM flow (Gardner & Lykoudis 1971). It is interesting to remark that the singular behaviour observed for $B = 0.33$ T is confined to a rather narrow range of the magnetic-field intensity values ($0.21 \text{ T} < B < 0.58$ T). We should also note that the intermittency is not due to instability of the injector itself – as proved by the stable results obtained by a slight increase (or decrease) of the magnetic field.

It might appear that the asymmetric void-fraction profile detected at $B = 0.3$ T is a singular case, characteristic to a certain entrance configuration, and that symmetric void-fraction profiles would otherwise be obtained. This is not, however, the case. In more recent experiments (Kirk 1984) with similar flow conditions but with different injector arrangements, attempts were made to achieve axisymmetric

† The length of these periods would require a longer averaging time. Since the averaging time was kept the same as for lower B-values, the intermittency resulted in the apparent data scatter observed for $B = 0.3$ T. (See Gherson (1981) for more details.)

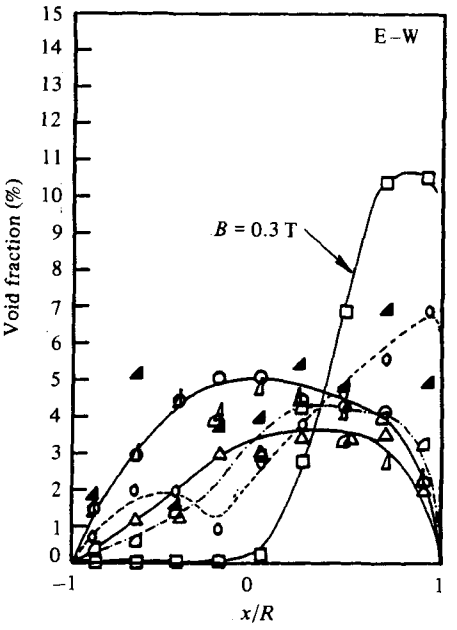

FIGURE 15. x-axis profiles of the local void fraction for gradually increasing magnetic field B (T): ○, 0; ◿, 0.085; ◢, 0.213; □, 0.330; ○, 0.580; ◿, 0.80; △, 0.94.

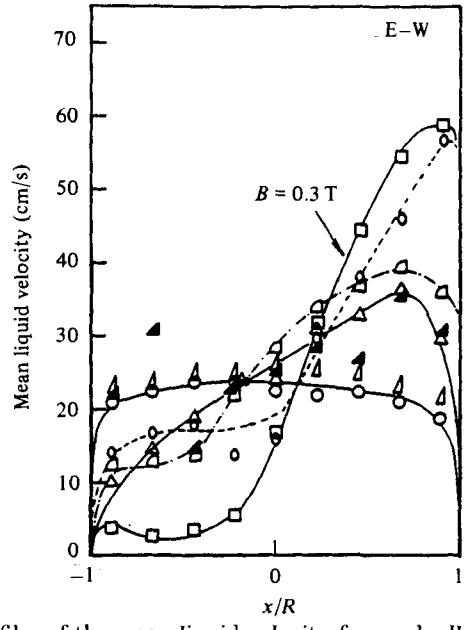

FIGURE 16. x-axis profiles of the mean liquid velocity for gradually increasing magnetic field. Symbols as for figure 15.

void distributions when the magnetic field was imposed. The first attempt was based on compensation of the asymmetry by intentionally biasing the gas injection, which was done by controlling each of the 10 injectors individually. It was found that symmetric profiles could not be obtained in this manner; the effect of slight changes in the gas injection was to cause the peak to shift to the opposing half of the test

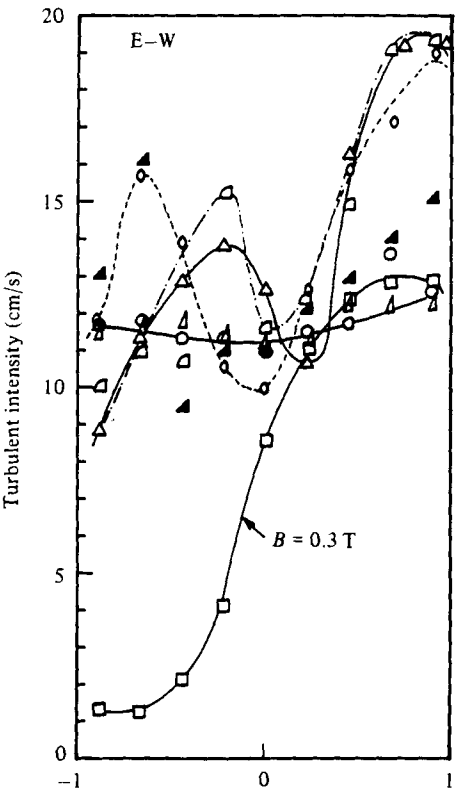

FIGURE 17. x-axis profiles of the turbulent intensity for gradually increasing magnetic field. Symbols as for figure 15.

section. In a later experiment, the nitrogen injection was modified considerably to include a flow-straightening section to suppress the secondary flows from the entrance bend. Even with the precautions taken to ensure the symmetry of the gas injection, the off-centre peaks persisted at magnetic fields in the neighbourhood of 0.3 T.

All of the above observations did not explain why a magnetic field higher than 0.3 T evened out the mean void profile. The explanation needs to be sought in the fact that as the magnetic field increases, the ponderomotive force redistributes the void fraction, leading to the formation of zones with large bubbles, which eventually break up as a result of their weaker surface tension. Evidence of this break-up can be found in figure 12, in the region $x/R > 0.5$, where the size of the bubbles detected at $B = 0.9$ T is, by a factor of roughly two, smaller than at $B = 0.3$ T. The additional turbulence associated with the break-up process is thought to promote the bubble mixing, allowing the bubble distribution to return to a shape similar to that found in the absence of the magnetic field. Without a systematic study involving controlled bubbles size at different magnetic-field intensities, it is hard to forward, at this time, a quantitative argument supporting this effect. Such an investigation has been attempted by Kirk and the results are available in his (1984) M.Sc. thesis (see also Lykoudis 1984). Preliminary experiments conducted by Kirk in the same facility have offered visual observation of the bubble break-up, at least for those bubbles that are seen rising on the Plexiglass wall. These visual observations, limited as they are by the surface-tension forces involving the solid wall, are consistent with our conclusion; namely that the bubble break-up mechanism starts occurring when the magnetic field is higher than 0.3 T.

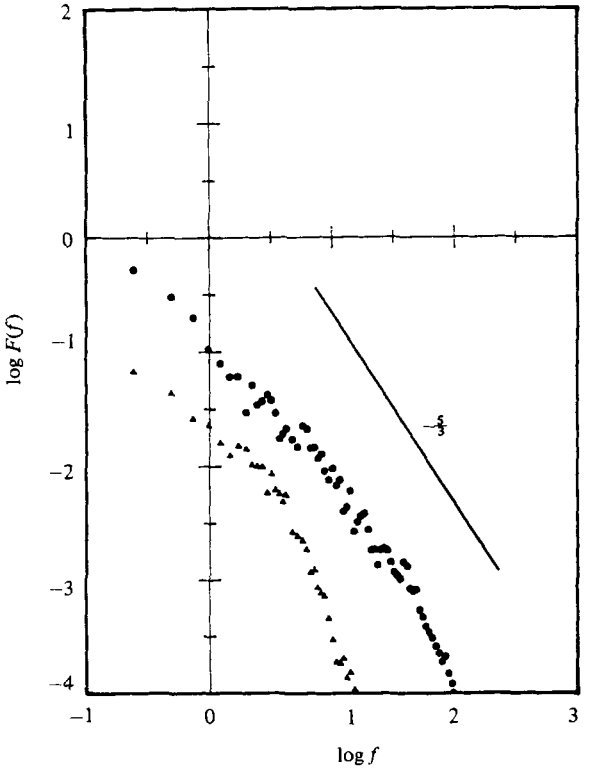

FIGURE 18. Frequency spectra for single-phase mercury flow at centreline. B (T): ●, 0; ▲, 0.3. Note change of key from previous figures.

4.4. *Magnetic-field influence on the turbulence spectra*

A set of preliminary measurements was taken in single-phase mercury flow ($Re = 63000$). The turbulence spectra obtained at the centreline and at $x/R = 0.88$ (on a diameter perpendicular to the magnetic field) are shown in figures 18 and 19. The corresponding spectra for a magnetic-field intensity $B = 0.3$ T are presented in the same figures. The zero-field spectra show essentially the same features as the spectra measured by Gardner & Lykoudis (1971) in mercury pipe flow, at $Re = 52000$, centreline and $x/R = 0.9$. A region with a slope of $-\frac{5}{3}$ is present over about one decade for the centreline data, but is less obvious in the spectrum mesured near the wall, which exhibits a steeper slope in the higher range of the frequencies. Another similar feature is that the turbulence suppression of the lowest-frequency components is more effective at the centreline than at the wall.

The salient feature of the spectra measured at the centreline in two-phase flow, at $Re = 63000$, is higher intensity over the whole frequency range than the corresponding single-phase spectrum (compare figures 18 and 20). We notice that, while in single-phase flow a magnetic field of 0.3 T reduced the spectral amplitudes by about one decade (see figure 18), a much smaller reduction is obtained in two-phase flow, even for a stronger magnetic field ($B = 0.9$ T, figure 20). This is due to the fact that the magnetic field cannot stop the bubbles from rising, so that the kinetic energy imparted to the fluid by the bubble movement is continuously feeding the turbulence, counteracting the suppressing effect of the magnetic field. Expressed in a different way, the Reynolds and Hartmann numbers are no longer the only parameters that determine the intensity of the turbulent fluctuations: in two-phase flow the latter

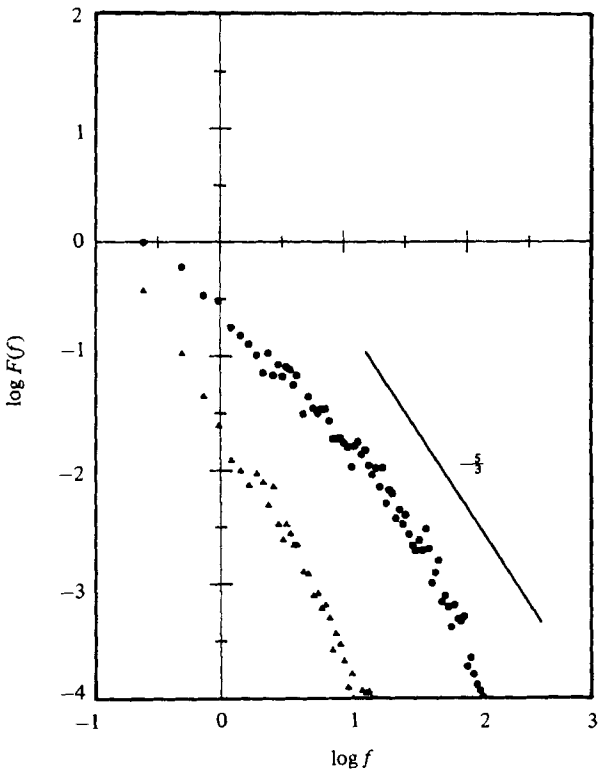

FIGURE 19. Frequency spectra for single-phase mercury flow at $r/R = 0.88$. Symbols as for figure 18.

depends also on the local void fraction at the considered location. It is worth mentioning here that the size of the bubbles (voids) affects the shape of the turbulent-fluctuation spectra. Larger size voids have been found (Gherson 1981) to produce higher amplitudes in the low-frequency range of normalized spectra.

The 'inertial subrange' in the two-phase case seems to be extended over a broader range of frequencies (two decades) than in single-phase flow spectra. This indicated a broader span separating the turbulence large scale from the dissipation scale. Since the ratio of these two scales is known (Hinze 1975) to be proportional to the turbulence Reynolds number based on the Taylor microscale and the turbulent intensity, the broader span is in agreement with the higher value of u' measured in two-phase flow with respect to the single-phase case.

The influence of the local void fraction on the ability of the magnetic field to suppress the turbulent fluctuations in the pipe is apparent in the measurements done near the pipe wall ($x/R = 0.88$, figure 21). A magnetic field $B = 0.3$ T would be expected, based on the single-phase measurements (see figure 19), to reduce the spectral amplitudes significantly, at all frequencies. However, owing to the increase in local void fraction caused by the presence of the field (from about $\alpha = 0.02$ to $\alpha = 0.10$) the latter was not able to suppress the turbulent fluctuations. Moreover, the amplitude of the turbulence spectrum increased in the higher frequency range ($f > 20$ Hz). The restructuring of the void distribution, when the magnetic field was increased to $B = 0.9$ T, changed the local void fraction to less than $\alpha = 0.01$ (see figure 8). The turbulence spectrum for this magnetic field exhibits lower amplitudes, with the exception of the lowest end of the frequency range, where no significant change in amplitude is observed.

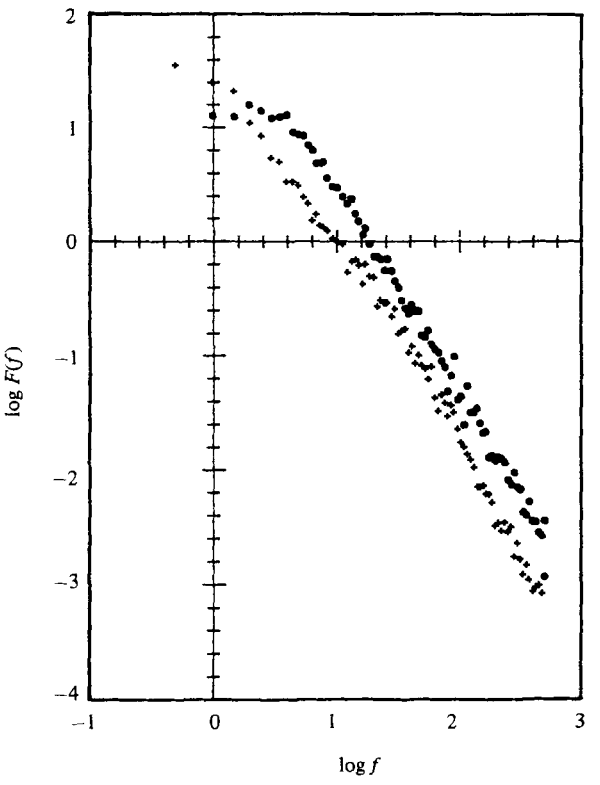

FIGURE 20. Frequency spectra in two-phase pipe flow at centreline, $\langle\alpha\rangle \approx 0.03$. B (T): ●, 0; +, 0.9.

The spectra for the above location ($x/R = 0.88$) exhibit a slope of about $-\frac{5}{3}$ for $B = 0$; the slope is seen to decrease slightly at $B = 0.3$ T, when the local void fraction is significantly higher and to increase to about -2.5 at $B = 0.9$ T (see figure 21).

The above discussion of the turbulent-frequency spectra at different positions has to be considered, with the caution that the spectral distribution depends not only on the magnetic-field intensity but also on the local values of void fraction and void size, and the complex flow pattern makes it very difficult to single out the influence of each one of the above factors.

The statistical description of the turbulent flow pattern would be more complete if it included the behaviour of the turbulent length-scales. In the absence of spatial cross-correlation measurements, the lengthscale computation relies on finding the appropriate 'convection velocity,' in the assumption that Taylor's hypothesis is valid for the considered flow field. In our experimental conditions, however, Taylor's hypothesis does not hold owing to the strong inhomogeneity of the flow, on one hand, and to the high level of the relative turbulent intensity (see e.g. Hinze 1975) on the other. These considerations point out the need for spatial cross-correlation measurements to allow the determination of the local values of the turbulent lengthscales.

5. Conclusions

The main result of the present work is the fairly complete set of data obtained, in the two-phase pipe flow, using a hot-film and a double conductivity probe. The following general conclusions stem from the analysis of this set of data.

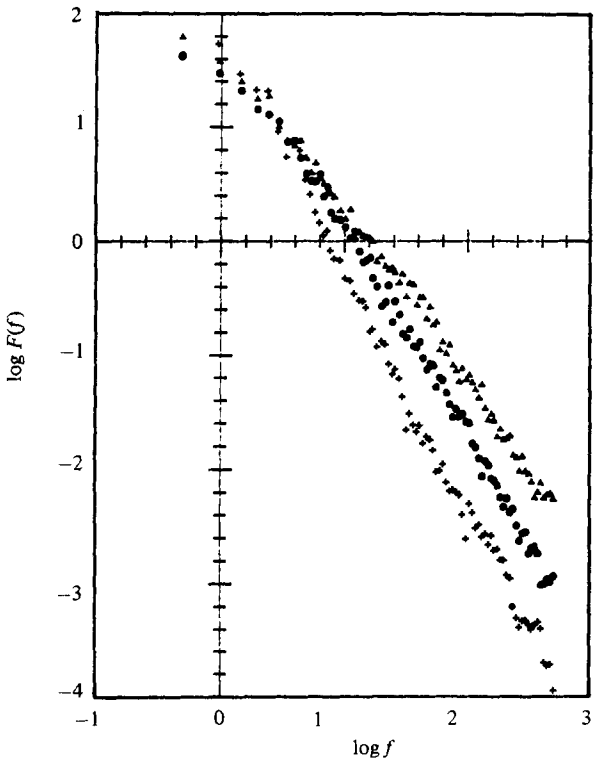

FIGURE 21. Frequency spectra in two-phase pipe flow, at $r/R = 0.88$, $\langle\alpha\rangle \approx 0.03$. B (T): ●, 0; ▲, 0.3; +, 0.9. α_{local}: ●, 0.02; ▲, 0.10; +, 0.005.

(*a*) The influence of a transverse magnetic field on a liquid-metal two-phase flow stresses any asymmetry existent in the entrance (mixer) region, by suppressing the mixing effect due to bubble agitation.

(*b*) As the magnetic field increases, the ponderomotive force redistributes the void fraction, leading to the formation of zones with large bubbles, which eventually break up as a result of their weaker surface tension. The additional turbulence associated with the break-up process is thought to promote the bubble mixing, allowing the bubble distribution to return to a shape similar to that found in the absence of the magnetic field.

(*c*) The suppression of bubble agitation seems to be associated with a critical value of the M/Re ratio, similar to the critical value well known in single-phase MFM flows. Intermittency effects were observed.

(*d*) The suppression, by the magnetic field, of turbulent fluctuations in the liquid phase is dependent upon the local void fraction present at the considered position. For the same local void fraction, the higher-frequency fluctuations are more readily suppressed than the ones of a lower frequency.

(*e*) Although, in a bubbly-flow regime, the presence of a transverse magnetic field diminishes the rising velocity of the bubbles, the corresponding change in the mean liquid velocity is such as to lead to an increase in the gas–liquid slip ratio.

As is known from single-phase MFM flows, the influence of the magnetic field on a flow in a cylindrical duct is more difficult to characterize than the flow in a quasi-two-dimensional geometry. Measurements in a high-aspect-ratio rectangular-cross-section channel are therefore highly desirable. The results of such measurements

could lead, for instance, to a quantitative correlation between the turbulence suppression by the magnetic field and the local parameters of the gas phase. The same two-dimensional geometry would facilitate the study of the magnetic entrance effects in a two-phase MFM flow, effects about which no data are presently available. A high-aspect-ratio rectangular test section, capable of yielding such data, is now available at our laboratory. The local measurements to be undertaken in this test section, using the hot-film anemometry and the data-processing techniques developed during the present work, will contribute to the knowledge of the magnetic-field influence on the liquid-metal–gas two-phase flow.

REFERENCES

ALEMANY, A., MOREAU, R., SULEM, P. L. & FRISCH, V. 1979 Influence of an external magnetic field on homogeneous MHD turbulence. *J. Méc.* **18**, 278–319.

BRANOVER, H. 1978 *Magnetohydrodynamic Flow in Ducts.* Wiley.

BRANOVER, H., HUNT, J. C. R., PROCTOR, M. R. E. & PIERSON, E. S. 1979 Magnetohydrodynamic flows and turbulence: a report on the Second Bat-Sheva Seminar, *J. Fluid Mech.*, **91**, 563–580.

DELHAYE, J. M. 1969 Two-phase flow instrumentation. In *Proc. 11th Natl ASME/AIChE Heat Transfer Conf. Minneapolis*, p. 58.

FABRIS, G., DUNN, P. F., GAWAR, J. Z. & PIERSON, E. S. 1980 Local measurements in two-phase liquid-metal MHD. In *MHD-Flows and Turbulence II* (ed. H. Branover & A. Yakhot), pp. 157–171. Israel Universities Press.

FERRARO, V. C. A. & PLUMPTON, C. 1966 *An Introduction to Magneto-Fluid-Mechanics.* Oxford University Press.

GARDNER, R. 1969 Magneto-fluid-mechanic pipe flow in a transverse magnetic field with and without heat transfer. Ph.D. thesis, Purdue University, West Lafayette.

GARDNER, R. & LYKOUDIS, P. S. 1971 Magneto-fluid-mechanic pipe flow in a transverse magnetic field. Part 1. Isothermal flow. *J. Fluid Mech.* **47**, 737–764.

GHERSON, P. 1981 Local measurements in a liquid-metal two-phase flow under the influence of a magnetic field. Ph.D. thesis, Purdue University, West Lafayette.

GHERSON, P. & LYKOUDIS, P. S. 1981 Hot film anemometry in a two-phase (liquid-Metal–Gas) medium. In *Proc. 7th Symp. on Turbulence, Univ. Missouri–Rolla, 21–23 September*, pp. 192–200.

HINZE, J. O. 1975 *Turbulence*, 2nd edn. McGraw-Hill.

HUNT, J. C. R. & MOREAU, R. 1976 Liquid metal magnetohydro-dynamics with strong magnetic fields: A report on Euromech 70. *J. Fluid Mech.* **78**, 271–288.

HUNT, J. C. R. & SHERCLIFF, J. A. 1975 Magnetohydrodynamics at high Hartmann number. *Annu. Rev. Fluid Mech.* **3**, 37–62.

KIRK, T. 1984 Experiments in liquid-metal two-phase magneto-fluid-mechanic pipe flow. M.Sc. thesis, Purdue University, West Lafayette.

LANCE, M., MARIE, J. L., CHARNAY, G. & BATAILLE, J. 1980 Turbulence structure of a co-current air–water bubbly flow. In *Proc. ANS/ASME/NRC Int. Topical Meeting on Nuclear Reactor Thermal Hydraulics*; *NUREG/CP*-0014, vol. 3, pp. 1363–1383.

LIELAUSIS, O. 1975 Liquid-metal magnetohydrodynamics. *Atomic Energy Rev.* **13**, 527–580.

LYKOUDIS, P. S. & DUNN, P. F. 1973 Magneto-fluid-mechanic heat transfer from hot-film probes. *Intl J. Heat Mass Transfer* **61**, 1439–1452.

LYKOUDIS, P. S. 1984 Liquid-metal magneto-fluid-mechanic turbubblence. Presented at the 4th Beer-Sheva Seminar on MHD Flows and Turbulence, Ben-Gurion University of the Negev, Beer-Sheva, Israel, 27 Feb.–2 Mar. 1984.

MALCOLM, D. G. 1976 Hot-film anemometry in liquid-metal MHD. In *MHD-Flows and Turbulence* (ed. H. Branover), pp. 119–123. Israel Universities Press Halsted.

MALCOLM, D. G. & VERMA, V. 1981 Dynamic response of forced convective heat transfer from hot-film to mercury. Part 2. Experiment. *J. Fluid Mech.* **112**, 475–485.

MICHIYOSHI, I., FANAKAWA, H., KURAMOTO, C., AKITA, Y. & TAKAHASHI, O. 1977 Local properties of vertical mercury–argon two-phase flow in a circular tube under transverse magnetic field. *Intl J. Multiphase Flow* **3**, 445–457.

MORI, Y., HIJIKATA, K. & KURIYAMA, I. 1976 Experimental study of bubble motion in mercury with and without magnetic field. Presented at the Winter Annual Meeting of ASME, Heat Transfer Division, New York, 5 December (*ASME* 76-WA/HT-65).

NEAL, L. G. 1963 Local parameters in co-current mercury–nitrogen flow. *Argonne Natl Lab. Rep.* ANL–6625.

OHBA, K. & YUHARA, T. 1979 Study of turbulence structure in a vertical square duct flow of a bubbly mixture using LDV, Presented at the 2nd Multiphase Flow and Heat Transfer Symposium Workshop, 16–18 April, Miami.

REED, C. & LYKOUDIS, P. S. 1978 The effect of a transverse magnetic field on shear turbulence. *J. Fluid Mech.* **89**, 147–171.

RESCH, F. J. & ABEL, R. 1975 Spectral analysis using Fourier transform techniques. *Intl J. Numer. Meth. in Engng* **9**, 869–902.

RESCH, F. J. & LEUTHEUSSER, J. H. 1972 Le ressault hydraulique: mesures de turbulence dans la region diphasique. *Houille Blanche* **4**, 279–293.

SAITO, M. 1978 Electrical and fluid dynamic characteristics in two-phase liquid metal MHD power generator. Ph.D. thesis, Osaka University.

SAITO, M., NAGAE, H.,INOUE, S. & FUJII-E, Y. 1978 Redistribution of gaseous phase of liquid-metal two-phase flow in a strong magnetic field. *J. Nucl. Sci. Technol.* **15**, 729–735.

SERIZAWA, A. 1974 Fluid-dynamic characteristics of two-phase flows. Ph.D. thesis, Institute of Atomic Energy, Kyoto University.

SERIZAWA, A., KATAOKA, I. & MICHIYOSHI, I. 1975 Turbulence structure of air–water bubbly flow: I – Measuring techniques; II – Local properties; III – Transport properties. *Intl J. Multiphase Flow* **2**, 221–259.

SHERCLIFF, J. A. 1975 *A Textbook of Magnetohydrodynamics*. Cambridge University Press.

THEOFANOUS, T. G. & SULLIVAN, J. 1982 Turbulence in two-phase dispersed flows. *J. Fluid Mech.* **116**, 343–362.

THOME, R. J. 1964 Effect of a transverse magnetic field on vertical two-phase flow through a rectangular channel. *Argonne Natl Lab. Rep.* ANL-6854.